# Molecular architecture of a network of potential intracellular EGFR modulators

# involving the juxtamembrane segment, ARNO, phospholipids and CaM

4 Aldino Viegas<sup>1,2,a#</sup>, Dongsheng M. Yin<sup>3,4#</sup>, Jan Borggräfe<sup>1,2,5</sup>, Thibault Viennet<sup>1,2,b</sup>, Marcel Falke<sup>1</sup>, Anton Schmitz<sup>3,4\*</sup>, Michael

5 Famulok<sup>3,4</sup>, Manuel Etzkorn<sup>1,2,5,6\*</sup>

6 7

8

2

3

- <sup>1</sup> Institute of Physical Biology, Heinrich-Heine-Universität Düsseldorf, Universitätsstr. 1, 40225 Düsseldorf, Germany
- <sup>9</sup> Institute of Complex Systems (ICS-6), Forschungszentrum Jülich, Wilhelm Jonen Strasse, 52425 Jülich, Germany
- <sup>3</sup> Max Planck Fellow Chemical Biology, Center of Advanced European Studies and Research (caesar), Ludwig-Erhard-Allee 2,
- 53175 Bonn, Germany
- <sup>4</sup> Department of Chemical Biology, Life and Medical Sciences (LIMES) Institute, Rheinische Friedrich-Wilhelms-Universität
- Bonn, Gerhard-Domagk-Str.1, 53121 Bonn, Germany
- <sup>5</sup> JuStruct: Jülich Center for Structural Biology, Forschungszentrum Jülich, Wilhelm Jonen Strasse, 52425 Jülich, Germany
- <sup>6</sup> Lead contact

16 17

18

19

- # equal contribution
- **Corresponding Authors**
- \*E-mail: anton.schmitz@uni-bonn.de
- \*E-mail: manuel.etzkorn@hhu.de

21 22

- Present Addresses
- <sup>23</sup> UCIBIO-REQUIMTE, Departamento de Química, Faculdade de Ciências e Tecnologia, Universidade Nova de Lisboa, 2829-516 Caparica,
- 24 Portugal
  - <sup>b</sup> Dana-Farber Cancer Institute, Cancer Biology, 360 Longwood Ave, Boston, MA 02215, USA

2627

28

29

30

31

32

33

34

35

36

37

25

### Summary

Epidermal growth factor receptors (EGFRs) are central cellular signaling interfaces whose misregulation is related to several severe diseases. While ligand binding to the extracellular domain is the most obvious regulatory element, also intracellular factors can act as modulators of EGFR activity. The juxtamembrane (JM) segment seems to be the receptor's key interaction interface of these cytoplasmic factors. However, only a limited number of cytoplasmic EGFR modulators are known and a comprehensive understanding of their mode of action is lacking. Here, we report ARNO, a member of the cytosine family, as another JM-binding protein and structurally characterize the ARNO-EGFR interaction interface. We reveal that its binding mode displays common features and distinct differences with JM's interaction with Calmodulin and anionic phospholipids. Furthermore, we show that each interaction can be modulated by additional factors, generating a distinctly regulated network of possible EGFR modulators acting on the intracellular domain of the receptor.

38 39

Keywords: ARNO-Sec7, Cytohesins, EGFR, Juxtamembrane, NMR

## Introduction

The epidermal growth factor receptor (EGFR) is a major regulator of proliferation in epithelial cells. Since its misregulated activation can lead to hyperproliferation and the development of cancer, an intricate regulatory network to control EGFR activity has evolved comprising systemic and cell-autonomous elements (Citri and Yarden, 2006). Key to the regulation of EGFR activity is the receptor's intrinsic autoinhibition, on which the regulatory network is built. The importance of this autoinhibition is evident from several mutations which disrupt the autoinhibition and are linked to specific types of cancer (Lemmon et al., 2014). In general, the autoinhibited state can be released by formation of an asymmetric EGFR dimer in which one kinase domain activates the other one (Zhang et al., 2006). This asymmetric dimer is stabilized by the juxtamembrane (JM) segments of both intracellular domains of the involved monomers. The C-terminal part of the JM segment of the activated kinase functions as a "latch" or "cradle" for the activator kinase (Jura et al., 2009; Red Brewer et al., 2009). In addition, the N-terminal parts of both JM segments are thought to form an antiparallel coiled-coil enhancing the affinity of the monomers for each other (Jura et al., 2009). The formation of the antiparallel coiled-coil requires the C-termini of the transmembrane helices to be separated from each other which on its turn is coupled to the ligand-bound conformation of the extracellular domain and thus confers regulation by EGF. In the inactive state, the basic JM segment binds to acidic phospholipids of the inner leaflet of the plasma membrane, and this interaction contributes to the autoinhibition of the receptor (Sengupta et al., 2009).

In addition to its function in relaying the conformational changes induced by EGF-binding from the extracellular domains to the kinase domains, the JM segment is a site of modulation of EGFR activity by intracellular factors. Previous studies identified a number of hot spots associated e.g. with kinase interaction (T654 and T669) (Hunter et al., 1984; Morrison et al., 1993), activation of the receptor (V665 and L680) (Red Brewer et al., 2009) or a possible conformational constraining of the receptor (R645 – R657) (Poppleton et al., 1999). When e.g. threonine-654 in the JM segment is phosphorylated by protein kinase C the activity of the EGFR is attenuated (Cochet et al., 1984; Davis and Czech, 1985; Friedman et al., 1984; Hunter et al., 1984) probably due to inhibition of EGFR dimerization (Thiel and Carpenter, 2007). Phosphorylation of another threonine (T669) in the JM segment by extracellular signal-regulated kinase (ERK) reduces EGFR downregulation (Li et al., 2008). Recently the tumor necrosis factor receptor associated factor 4 (TRAF4) has been reported to interact with the C-terminal part of EGFR-JM to promote receptor dimerization (Cai et al., 2018). The cytosolic protein calmodulin (CaM) binds to the N-terminal part of the JM segment in a calcium-dependent manner (Aifa et al., 2002; Martin-Nieto and Villalobo, 1998) enhancing EGFR activation (Li et al., 2012; McLaughlin et al., 2005).

In this work we report on the ability of ARNO (ADP ribosylation factor nucleotide binding-site opener), a member of the cytohesin family of guanine nucleotide exchange factors, to bind EGFR's JM domain. While ARNO has been proposed to function as activator of the EGFR (Bill et al., 2012; Pan et al., 2014; Pan et al., 2013), the underlying mechanism has not been determined. Here, we provide a comprehensive in vitro analysis of the determinants that define the ARNO-JM interaction and characterize the interaction at the molecular level in the absence and presence of a membrane environment. We identify the JM-binding site in the Sec7 domain of ARNO and show that JM's interaction with ARNO-Sec7 displays large similarities to its interaction with CaM, pointing to the speculation that ARNO and CaM may modulate EGFR in a similar manner. Our data also reveal that ARNO-Sec7, CaM as well as lipid bilayers containing anionic phospholipids compete for overlapping binding sites on the JM segment. Moreover, we show that additional factors including auto inhibition for ARNO, Ca<sup>2+</sup> availability for CaM and lipid composition for JM's membrane association, are capable to further regulate this competitive network of EGFR-

JM interaction partners. While we here focus on the structural and biophysical characterization of this network under defined in vitro conditions, our findings are consistent with previous findings in living cells and in tumor tissue (Bill et al., 2012; Pan et al., 2014; Pan et al., 2013) and should stimulate future studies of this important aspects in EGFR signaling.

### **Results and Discussion**

## The JM segment of the EGFR interacts with the Sec7 domain of ARNO

To investigate whether ARNO interacts with the EGFR we carried out microscale thermophoresis (MST) measurements of selected isolated domains. Since ARNO is a cytosolic protein, only EGFR constructs comprising the intracellular domain were considered (Fig. 1a). Our MST data show that the EGFR intracellular domain (ICD) indeed interacts with the Sec7 domain of ARNO (Sec7) (Fig. 1b, black). The other major domain of ARNO, the pleckstrin homology domain (PH), did not show binding under the applied conditions (data not shown). Interestingly the purified juxtamembrane segment (JM) alone displays a comparable binding behavior to ARNO-Sec7 as EGFR-ICD (Fig. 1b, blue). While EGFR-ICD and EGFR-JM bind ARNO-Sec7 with similar affinity ( $K_D$  of about 50  $\mu$ M), an EGFR-ICD construct lacking the first 27 amino acids of the JM segment (EGFR-ICD $\Delta$ JM<sub>1</sub>. 27) does not show interaction (Fig. 1c, grey), which is also true for a scrambled version of JM (JMsc) containing the same amino-acids, but randomly redistributed (Fig. 1c, pink, see Methods for full sequence). Our data demonstrate that ARNO-Sec7 interacts with the EGFR *in vitro* and strongly suggest that this interaction is on the EGFR side mainly driven by the JM segment.

Due to JM's key role in EGFR regulation (Doerner et al., 2015; He and Hristova, 2012; Jura et al., 2009; Poppleton et al., 1999; Red Brewer et al., 2009; Thiel and Carpenter, 2007) and its high potential for EGFR signaling modulation (Aifa et al., 2002), we carried out a comprehensive NMR study to characterize the molecular architecture of the interaction of ARNO-Sec7 and EGFR-JM. Following the full resonance assignments of both domains (see Methods Table 1 and 2 and Fig. S1 for details on data acquisition, resonance assignment and structural features) we performed NMR-based titration studies with Sec7 and JM to identify the interacting regions based on the chemical shift perturbations (CSP) induced by their binding partner. Figure 1d-g summarize the data from the point of view of the ( $^{15}$ N-isotope-labeled) JM segment. The presence of increasing amounts of (unlabeled) Sec7 induces characteristic concentration-dependent chemical shift perturbations for certain residues (Fig. 1d). Plotting these chemical shift perturbations along the JM sequence clearly identifies the N-terminal half of JM, i.e. the JM-A segment (Jura et al., 2009), as the one involved in the interaction with Sec7. Furthermore, the NMR chemical shifts continuously change with increasing concentration of Sec7, revealing a rather transient interaction (NMR fast-exchange regime) with residue specific binding affinities ( $K_D$ ) in the high  $\mu$ M range (see Supporting information Fig. S1e for more details).

In general, NMR chemical shifts, in particular of carbon  $C\alpha$  and  $C\beta$  nuclei, are robust indicators of secondary structure (Berjanskii and Wishart, 2017). Analysis of the respective chemical shifts of the isolated JM segment points to the absence of a clear secondary structure when free in solution (Fig. 1f). This observation is in good agreement with previous results (Choowongkomon et al., 2005; Mineev et al., 2015) in which JM was shown to behave mainly as random coil in the absence of membrane mimetics.

Addition of Sec7 did not lead to detectable <sup>13</sup>C chemical shift perturbations (data not shown), which suggests that the interaction with Sec7 does not induce a stable secondary structure in JM. However, the rather uniform shift of the affected peaks in the <sup>1</sup>H, <sup>15</sup>N-HSQC spectrum (Fig. 1d) towards lower <sup>1</sup>H and <sup>15</sup>N frequencies would be in line with an increase in

transient  $\alpha$ -helical propensity upon Sec7 binding (Berjanskii and Wishart, 2017). The JM segment of EGFR contains a high number of charged residues (see Fig. S1c). In particular the JM-A segment comprises an unusually high number of positively charged residues (i.e. 9 out of 19 residues). To test whether the interaction with Sec7, which contains both negatively and positively charged regions (Fig. S2), is driven by nonspecific electrostatic interactions we used again the scrambled JM construct (JM<sub>SC</sub>) containing the same total amino acid composition but randomly redistributed. In line with the MST measurements (Fig. 1c, pink), the NMR measurement (using  $^{15}$ N-labeled JM<sub>SC</sub>, Fig. 1g) shows that the scrambled JM does not interact with Sec7, in clear contrast to wild-type JM under identical conditions (e.g. Fig. 1d, purple). Our data therefore demonstrate that the absolute charge of JM is not key to the interaction and imply that the primary sequence of JM promotes a specific recognition by Sec7.

Due to its good NMR properties (Betz et al., 1998) ARNO-Sec7 offers the appealing opportunity to investigate the interaction also from the cytohesin point of view. Consequently, we recorded a series of NMR experiments using <sup>15</sup>N-isotope labeled ARNO-Sec7 and non-labeled EGFR-JM (Fig. 2). In line with the data obtained from the JM point of view (Fig. 1), the presence of increasing amounts of EGFR-JM induced chemical shift perturbation for specific Sec7 residues (Fig. 2b,c) reproducing the transient interaction of the two domains (NMR fast exchange regime) and pinpointing a specific JM-binding site of Sec7. Following the resonance assignment of the 21 kDa Sec7 construct (Fig. S1, BMRB deposition code: 27761) distinct regions of the Sec7 domain can be identified that interact with the isolated JM segment (Fig. 2d). The affected residues mainly cluster around helices E (5), F (6), G (7), H (8) and I (9) and the loop connecting helices I (9) and J (10) (helix nomenclature as in (Mossessova et al., 1998) and, in brackets, according to (Betz et al., 1998)). Highlighting the most affected residues in the Sec7 structure reveals a well-defined JM-binding interface (Fig. 2e).

While the affected region partially overlaps with the negatively charged surface of Sec7 (see Fig. S2), it also involves a high number of hydrophobic residues (about 13 in the central binding interface of Sec7 and 7 in JM), suggesting that ARNO-Sec7 interacts with EGFR-JM, in part, through an extended hydrophobic surface. In particular, a surface-exposed hydrophobic patch of residues in Sec7's helix H appears to be in the center of this interaction. Reducing the hydrophobicity of this patch by alanine substitutions of Y186, F190, I193 and M194, i.e. ARNO-Sec7(4A), indeed inhibits binding to JM as determined by MST (Fig. 2f).

Of note, the observed binding site is also located in a region populated by residues crucial for the interaction of Sec7 with ARF1 (Betz et al., 1998; Cherfils et al., 1998; Mossessova et al., 1998). ARF1 binding is prevented in the autoinhibited state in all cytohesin members when helix H forms intramolecular contacts with the linker and the polybasic region (pbr). Accordingly, ARNO lacking the polybasic region (ARNOΔpbr) loses this autoinhibition (DiNitto et al., 2007). To test whether this autoinhibitory mechanism also plays a role for an interaction of ARNO with the EGFR, we carried out MST measurements using EGFR-ICD and either full-length ARNO or ARNOΔpbr (Fig. 2g,h). Indeed, full length (autoinhibited) ARNO did not bind EGFR-ICD (Fig. 2g, black) whereas for ARNOΔpbr the interaction was restored (Fig. 2g, green). This data supports the importance of Sec7's helix H in the interaction and suggests that ARNO's autoinhibitory mechanism may also regulate its interaction with the EGFR.

#### EGFR-JM's interaction with membranes shares common features and distinct differences to ARNO-Sec7

We have shown that ARNO-Sec7 binds the JM segment of the EGFR. As it is known that the JM segment also interacts with CaM and anionic phospholipids of the inner leaflet of the plasma membrane (Abd Halim et al., 2015; Aifa et al., 2002; Hedger

et al., 2015; Maeda et al., 2018; Sanchez-Gonzalez et al., 2010; Sengupta et al., 2009) we subsequently investigated similarities and/or differences in the binding mode of these interactors. To obtain the desired high-resolution information into the effect of the membrane surface, the interactions of JM with phospholipids in the form of phospholipid-bilayer nanodiscs (NDs) were characterized by NMR spectroscopy.

Our data show that the presence of NDs containing only the neutral POPC phospholipid does not induce noticeable chemical shift perturbations in EGFR-JM (Fig. 3a, yellow), indicating that this domain on its own does neither interact with neutral phospholipids nor with the membrane scaffold proteins (MSP) used to assemble the NDs. While the latter corroborates usage of MSP-derived nanodiscs as suitable membrane mimetic for the system, the absence of interactions with POPC lipids differs to previous findings in which a strong interaction of JM to DPC micelles was observed (Choowongkomon et al., 2005). Since DPC detergent molecules and POPC lipids both comprise the same phosphocholine head group, our results suggest that the overall assembly of the membrane mimetic (detergent-free lipid bilayers vs. detergent monomer-micelle equilibrium) has a strong influence on the interaction with JM. At this point it can only be speculated that the nanodiscs better reflect the physiologically-relevant membrane interaction of JM. However, in any case, the observed difference between detergent micelles and nanodiscs highlights the importance of the choice of a suitable membrane mimetic for structural studies of membrane interactions.

The strengths of the nanodisc system include its homogeneity, stability, the absence of detergents and near native bilayer arrangement as well as a the possibility to accurately change their lipid composition without modifying other parameters and use NMR-spectroscopy to determine lipid specific interaction with single amino acid resolution (Viegas et al., 2016; Viennet et al., 2018). In the following we made use of these features to investigate the interaction of JM with NDs containing 30% anionic phospholipids via NMR spectroscopy. Two different phospholipid mixtures were used, i.e. 30% anionic DMPG lipids with 70% neutral DMPC lipids as well as anionic POPS lipids (30%) with neutral POPC lipids (70%). In both cases clear changes in the NMR spectrum induced by the presence of the respective nanodiscs can be observed (Fig. 3a, Fig. S3 and Fig. S4). Similar to the interaction with ARNO-Sec7, the residues affected the most by the presence of the anionic membrane surface are confined to the JM-A region. However, a closer look also reveals that the phospholipid interacting region is a few residues shorter than the Sec7-binding region.

A comparison of the results obtained on the frequently used model phospholipids DMPC/DMPG (Fig. 3a, maroon and Fig. S4) to the more physiologically relevant POPC/POPS phospholipids (Fig. 3a, orange and Fig. S4) reveals that the observed effects are slightly elevated for the DMPC/DMPG system, suggesting that the different position of the negative charge in the head group and/or the presence of unsaturated fatty acids may affect the interaction with JM.

A comparison of EGFR-JM's interaction with anionic lipids or ARNO-Sec7 highlights four different sections in JM (Fig. 3b,c). While residues V650-Q660 show considerable chemical-shift perturbations induced by both interaction partners, the first half of these residues (V650-L655, Fig. 3c, section #1) show clearly different chemical shifts upon binding to lipids or Sec7, whereas the second half (R656-Q660, Fig. 3c, section #2) experience an almost identical variation in chemical shift. The third section (R662-V665, Fig. 3c, section #3) is only affected by Sec7 and not by the lipids. The fourth section (L667-I682, Fig. 3c, section #4) is not affect by the presence of either interaction partner. Consequently, EGFR-JM's interaction with anionic phospholipids shares some common features with the interaction with ARNO-Sec7, but also displays distinct differences. While the presence of NDs with 30% content of anionic phospholipids leads to chemical shift perturbations, indicative of fast exchange processes, increasing the membrane charge density to 50% anionic phospholipids alters the interaction kinetics

and leads to considerable peak broadening, indicative of intermediate exchange processes (see supplementary Fig. S4 for full experimental data). Considering the size of the ND system, a tight binding (in the slow exchange regime) could also explain this observation. In any case, it can be assumed that the JM-membrane interaction becomes stronger with increased negative charge density of the membrane. When plotting the peak intensity instead of the chemical shift changes it can be seen that also under these conditions, the JM-A region is the driving force of the interaction (Fig. 3d).

Overall our data shows that despite JM-A being mainly involved in the interaction with lipids and Sec7, the interaction with Sec7 occurs over an extended binding region that involves a number of additional JM residues, as compared to JM's interaction with the membrane surface. In addition, an increase of the anionic lipid content from 30% to 50% slows down the otherwise fast bound-to-free exchange processes, revealing the possibility of modulating JM's membrane interaction kinetics by variations in lipid composition.

#### The interplay of lipids, CaM and Sec7 as intracellular modulators of EGFR-JM

To directly compare the observed interaction of EGFR-JM with ARNO-Sec7 to the known cytoplasmic EGFR modulator CaM, we carried out additional MST and NMR-based experiments. Unsurprisingly, our MST data shows that binding of CaM to EGFR-ICD is calcium- and JM-dependent (Fig. 4a). When recording NMR spectra of EGFR-JM in the presence of unlabeled CaM, a set of peaks disappear from the spectrum (in line with an interaction in the NMR intermediate exchange regime). As expected (Aifa et al., 2002; Tebar et al., 2002), plotting the decrease in intensity along the JM sequence again reveals that predominantly JM-A interacts with CaM (Fig. 4b). Looking at the affected JM residues it can be seen that the CaM binding region of JM is again a few residues longer than its membrane binding region. Interestingly the CaM and the Sec7 binding regions of JM are essentially identical. However, in line with a higher binding affinity seen in the MST data ( $K_D$  of about 1  $\mu$ M), the NMR data also suggest that CaM interacts less transiently with JM as compared to Sec7 or membranes with 30% negative charge content.

Having found that CaM and ARNO-Sec7 bind to an essentially identical binding site on EGFR-JM we investigated a possible competition of CaM and ARNO-Sec7 for binding to the EGFR using MST. In line with the higher binding affinity of CaM, when EGFR-ICD (200 nM) was preincubated with a saturating concentration of CaM (30 μM), the binding of ARNO-Sec7 was completely prevented (Fig. 4c), confirming a competitive binding of CaM and ARNO-Sec7 *in vitro*.

Our data shows that CaM and ARNO-Sec7 interact with the same JM region. This fact hinders a reliable NMR investigation of the competition between these two proteins. In contrast, the binding regions of JM to phospholipid nanodiscs or Sec7 sufficiently differ to allow distinction between the binary JM-nanodisc and JM-Sec7 complexes. In particular, residues (E661-V665) in the center of the JM segment can be used as reporters since they are not affected by binding to phospholipids but are part of the Sec7-interacting region (Fig. 3b and S4). Indeed, when adding unlabeled ARNO-Sec7 to the JM peptide preincubated with NDs containing high amounts of anionic lipids (50/50% POPC/POPS) distinct chemical shift perturbations are visible for the 'Sec7-specific-reporter residues' E661-V665 as compared to free JM or to JM in the presence of just NDs (Fig. 5a and Fig. S4). The observed peak shift is consistent with the perturbations expected due to formation of a JM-Sec7 complex. Interestingly, JM residues directly at the edge of the membrane binding interface (Q660 and R662) show stronger or different chemical shift perturbation when both binding partners are present (as compared to the individual pairwise interactions, Fig 5a). This behavior is indicative of cooperative effects and/or different structural alterations. While our data does not allow to distinguish between a ternary JM-membrane-Sec7 complex or an exchanging 3-state equilibrium (free JM,

membrane-bound JM, Sec7-bound JM), the NMR data show that ARNO-Sec7 can interact with the JM peptide even in the presence of NDs containing a high amount of anionic lipids and thus support the notion that ARNO can interact with the EGFR at the plasma membrane.

### Conclusions

Using solution NMR spectroscopy and microscale thermophoresis (MST), supported by site-directed mutagenesis techniques, we show that ARNO-Sec7 and EGFR-JM interact *in vitro*. The residues of both Sec7 and JM involved in binding were identified (Fig. 1 and 2). From the JM side, NMR data showed that Sec7 specifically recognizes the first half of the segment (i.e. JM-A, Fig. 1e), which has been shown to be of importance for EGFR activation (Doerner et al., 2015; He and Hristova, 2012; Jura et al., 2009; Poppleton et al., 1999; Thiel and Carpenter, 2007). JM-A is also the region recognized by calmodulin (Fig. 4), a major regulatory protein of the EGFR (Aifa et al., 2002; Li et al., 2012; Sanchez-Gonzalez et al., 2010; Tebar et al., 2002). Furthermore, JM-A tethers JM to the plasma membrane (Fig. 3), stabilizing the inactive conformation of the EGFR (Arkhipov et al., 2013; Kovacs et al., 2015).

The isolated JM peptide in solution seems to exist mainly as random coil (Fig. 1f), with some propensity to form a transient  $\alpha$ -helix at the JM-A region (Arkhipov et al., 2013; Endres et al., 2013; Jura et al., 2009; Mineev et al., 2015). Our data reveals that, upon binding to Sec7, the amide resonances of JM-A shift upfield (Fig. S4c), which is indicative of a higher helical propensity in the Sec7-bound conformation. The JM segment also interacts with negatively charged phospholipids of the inner leaflet of the membrane (Kovacs et al., 2015; Sengupta et al., 2009). By using phospholipid nanodiscs (NDs) we demonstrate that JM-A is also the region responsible for binding to membranes containing anionic lipids. While the membrane-binding and Sec7-binding regions of JM largely overlap, a closer analysis of the NMR data shows that some residues experience different chemical shift perturbations upon binding to either partner and that the binding interface to Sec7 is elongated as compared to the lipid binding interface (Fig. 3b and Fig. S4).

From the Sec7 side, our data shows that the accessibility of the JM binding site is restricted when ARNO is in the autoinhibited state which is common to all cytohesin members (DiNitto et al., 2007) (Fig. 2). Release from the autoinhibition requires the binding of an already activated, membrane-attached ARF molecule or of phosphoinositides (PIPs) to the PH domain and maximum activation requires both steps resulting in exposure of the Sec7 domain (Cohen et al., 2007; Stalder et al., 2011). As PIPs cluster around the EGFR (Abd Halim et al., 2015; Hedger et al., 2015; McLaughlin et al., 2005; Michailidis et al., 2011; Wang et al., 2014), binding of ARNO to these PIPs would bring it near to the EGFR and simultaneously activate it for JM binding (see Fig. S5 for schematic visualization). The PIPs-driven co-localization and/or insufficient Ca<sup>2+</sup> availability could also counteract the higher affinity observed for Ca<sup>2+</sup>-activated CaM as possible competitor of the ARNO-EGFR interaction. The interplay between ARNO's expression level and state of activation, the plasma membrane's lipid composition and its arrangement, as well as the available Ca<sup>2+</sup>- and CaM levels could therefore provide a further layer of modulation of EGFR signaling (Fig. 5b).

Whether binding of ARNO to the JM segment of the EGFR occurs in the living cell and whether this binding would indeed modulate EGFR signaling is however currently unknown. There is indirect evidence for ARNO modulating EGFR activity (Bill et al., 2012; Pan et al., 2014; Pan et al., 2013) but the mechanism has not been elucidated. Due to our findings that *in vitro* ARNO interacts with the JM segment in a similar way as CaM does, it is tempting to speculate that ARNO and CaM could modulate EGFR activity also by a similar mechanism. Although the mechanism by which CaM modulates EGFR activity has

not yet been exactly determined, it appears to involve the weakening of JM's interaction with phospholipids of the membrane (McLaughlin et al., 2005; Sato et al., 2006; Sengupta et al., 2009). Our data obtained in the presence of phospholipid nanodiscs are consistent with this view and with a model in which CaM and ARNO could contribute to the activation of the EGFR by releasing one of several autoinhibition mechanisms of the EGFR, namely the immobilization of the JM segment on the surface of the membrane.

### **Author contributions**

Conceptualization, A.S, M.F. and M.E; Methodology, A.V., D.M.Y, A.S, M.F. and M.E.; Investigation, A.V., D.M.Y., J.B., T.V., and M.F.; Writing – original manuscript, A.V., A.S. and M.E.; Writing – Review & Editing, all authors; Funding Acquisition, A.V., M.F. and M.E.; Supervision, A.S., M.F., and M.E.

## Acknowledgements

We thank Y. Aschenbach and V. Fieberg for help with protein expression and purification. We acknowledge access to the
Jülich-Düsseldorf Biomolecular NMR Center. This work was supported by grants from the German Research Foundation (DFG)
(ET 103/2-1) to ME and from the European Union's Horizon 2020 research and innovation programme under the Marie
Sklodowska-Curie grant agreement N° 660258 to AV.

### **Declaration of Interests**

The authors declare no competing interests.

## **Abbreviations**

ARNO, ADP ribosylation factor nucleotide binding-site opener; CaM, Calmodulin; EGFR, Epidermal Growth Factor Receptor; ICD, Intracellular Domain; JM, Juxtamembrane; MST, Microscale Thermophoresis; NMR, Nuclear Magnetic Resonance.

## **Figures**

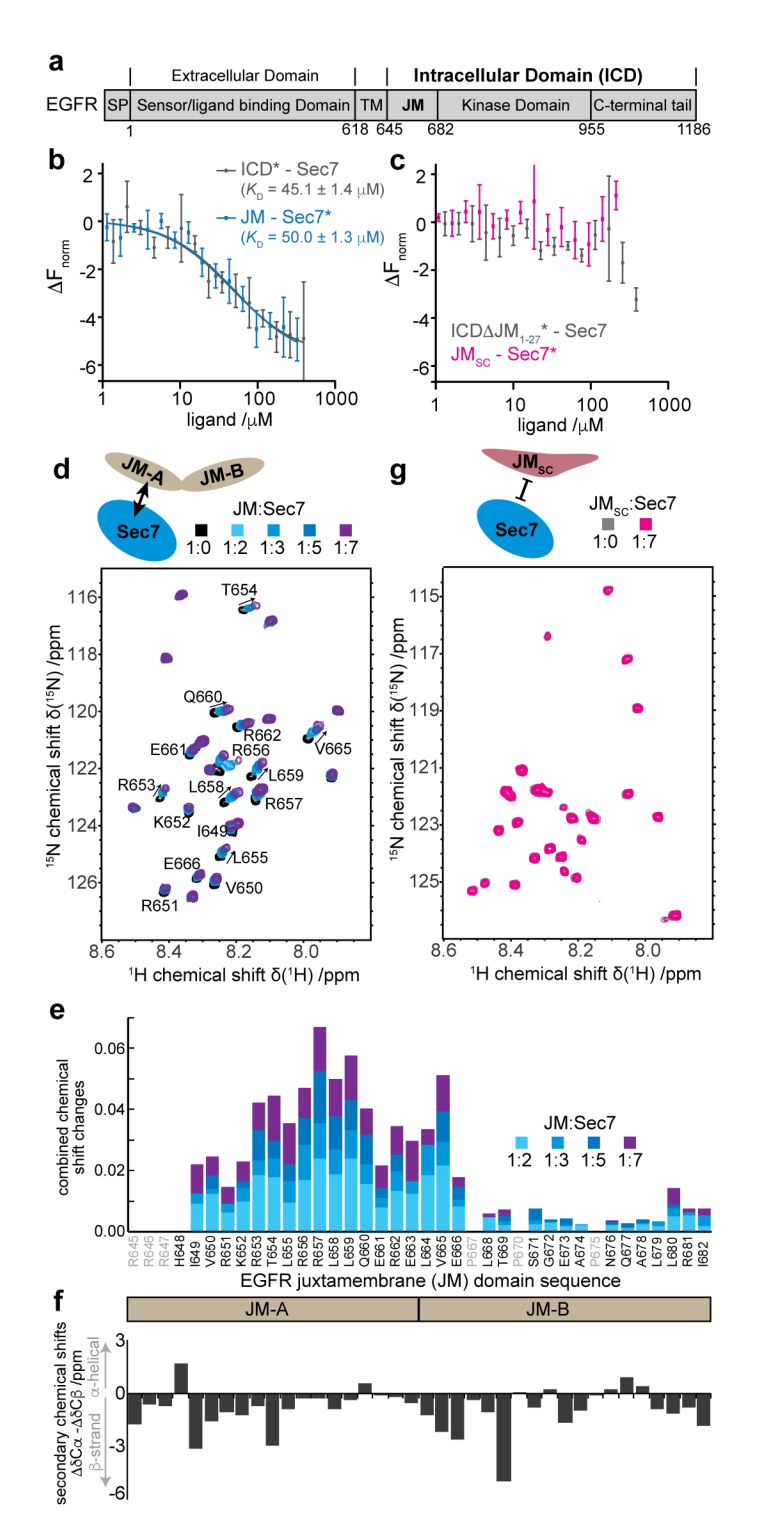


**Fig. 1. JM-Sec7 interaction as seen from the EGFR-JM side.** a) Schematic representation of EGFR's domain architecture (SP: signal peptide; TM: transmembrane domain; JM: juxtamembrane). b+c) MST data for indicated EGFR and ARNO constructs. Here and in the subsequent figures the EGFR construct is always mentioned first and the fluorophore-labeled molecule is labeled with asterisk (n=3, mean±SD). d) [¹H,¹⁵N]-HSQC NMR spectra of ¹⁵N-labeled EGFR-JM in the presence of increasing amounts of unlabeled ARNO-Sec7. e) Chemical shift perturbations along the EGFR-JM sequence induced by the presence of indicated amounts of ARNO-Sec7. Grey labels indicate residues that were not observed. f) Secondary chemical shifts (see Supplementary Information for definition) as indicator for secondary structure of EGFR-JM when free in solution. g) [¹H,¹⁵N]-HSQC NMR spectra of a ¹⁵N-labeled scrambled version of EGFR-JM (JM<sub>SC</sub>) in the absence (grey) or presence of 7-fold excess (magenta) of ARNO-Sec7.

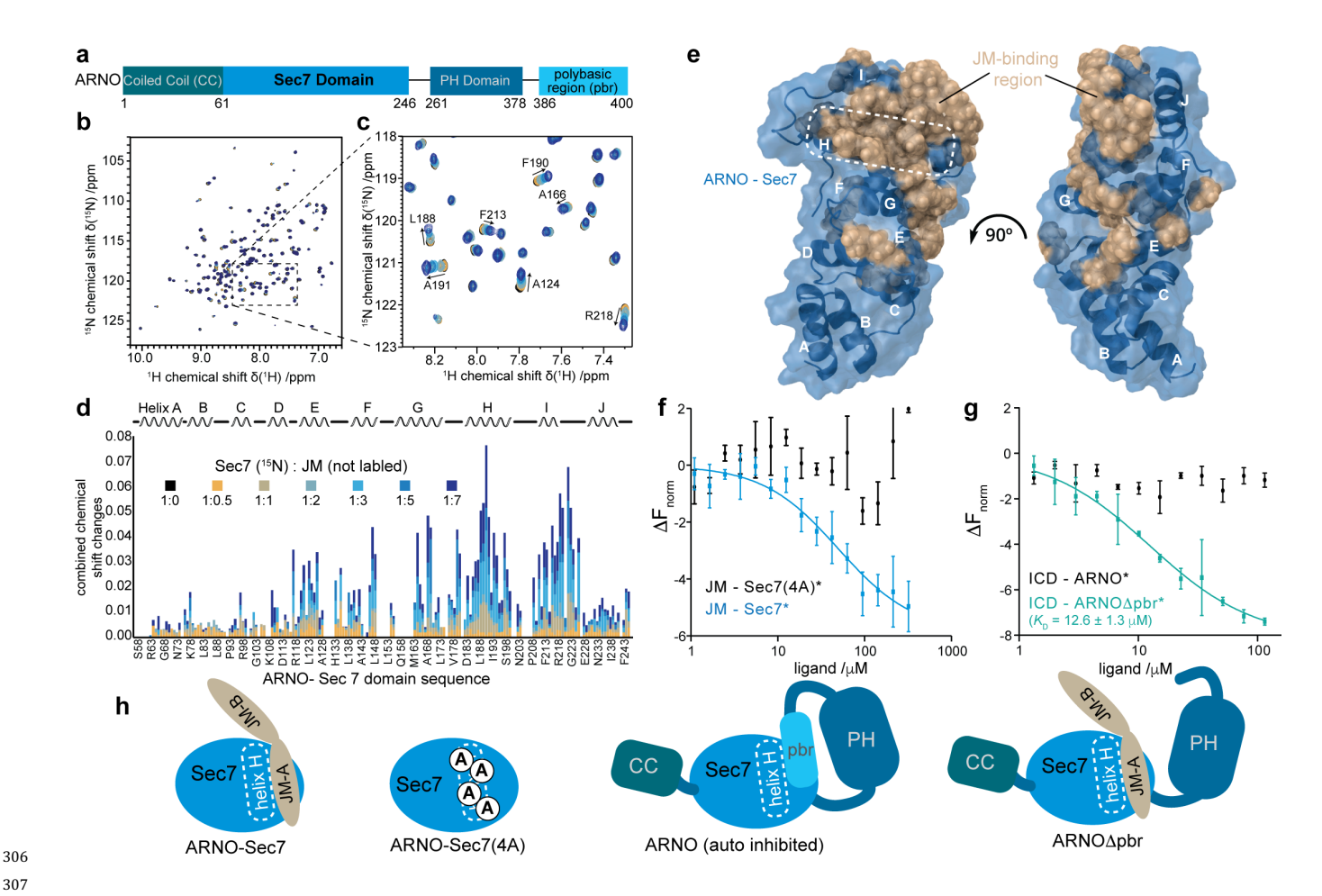


**Fig. 2. JM-Sec7 interaction as seen from the ARNO-Sec7 side.** a) Schematic representation of ARNO's domain architecture. b+c) [ $^1H$ , $^{15}N$ ]-HSQC NMR spectra of  $^{15}N$ -labeled ARNO-Sec7 in the presence of increasing amounts of unlabeled EGFR-JM (color code as in d). d) Chemical shift perturbations along the ARNO-Sec7 sequence induced by the presence of indicated molar ratios of EGFR-JM. e) Mapping of most affected residues on the 3D structure of ARNO-Sec7 (pdb code: 4JMI (Rouhana et al., 2013)) indicating the EGFR-JM binding site of ARNO-Sec7. f+g) MST data showing disruption of JM's interaction with ARNO-Sec7 due to mutations (f) or autoinhibition (g). f) Alanine substitutions of surface-exposed hydrophobic residues of helix H of Sec7, i.e. Sec7(4A), lead to disruption of the interaction with JM. The JM-Sec7 data (blue) is identical to data shown in Fig. 1b and serves as reference. g) While the presence of the autoinhibitory polybasic region (pbr) in full-length ARNO inhibits interaction with EGFR-ICD (black), deletion of the polybasic region (ARNOΔpbr) restores the interaction (n=3, mean $\pm$ SD). h) schematic summary of MST and NMR results.

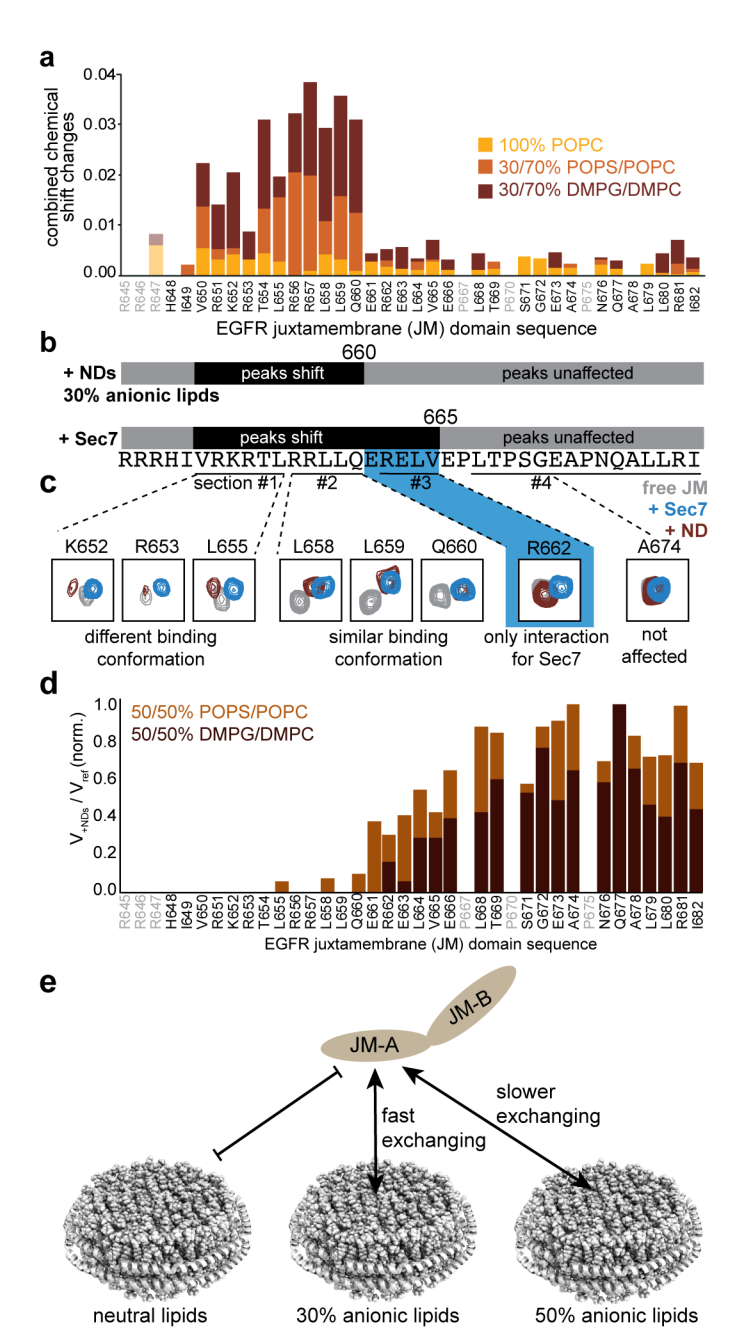


Fig. 3. JM-membrane interaction depends on anionic lipid content and follows a similar pattern as Sec7 binding with distinct differences. a) Chemical shift perturbations along the EGFR-JM sequence induced by the presence of nanodiscs with the indicated lipid composition. b) Schematic comparison of EGFR-JM binding behavior to lipid bilayers containing 30% anionic lipids (upper chart) or ARNO-Sec7 (lower chart, according to data shown in Fig. 1e). c) NMR signals of selected residues representative of JM regions with different behavior induced by the presence of Sec7 (blue peaks, also see Fig. 1) or NDs with 30% anionic lipids (red peaks). Blue area highlights residues showing interaction exclusively with Sec7 and not the used NDs. d) Effects of addition of NDs with 50% anionic lipid content. Unlike to the peak shifts visible for ND interaction with 30% anionic lipid content (a) or Sec7 binding (Fig. 1), addition of NDs containing 50% POPS and 50% POPC (brown) or 50% DMPG and 50% DMPC (dark brown) lipids predominantly leads to disappearance of peaks for residues in JM-A (see. Fig. S3 and S4 for comparison of spectra, peak shifts and volumes for all used lipid mixtures). The observed peak disappearance is indicative of prolonged contact times of this region with the lipids (i.e. NMR medium or slow exchange regime for 50 % anionic lipids and NMR fast exchange regime for 30 % anionic lipids or Sec7). e) Schematic summary of EGFR-JM's interaction with different NDs. In a) and d), grey labels indicate residues that were not observed.

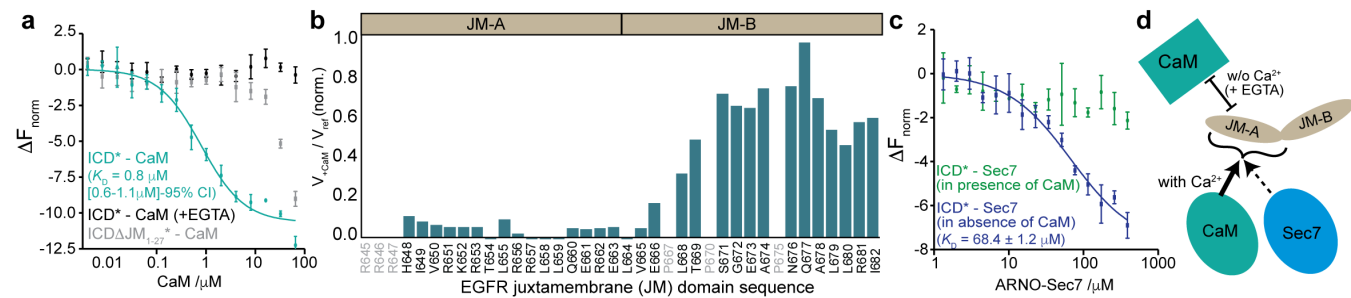


Fig. 4. Calmodulin (CaM) and ARNO-Sec7 share same binding site and compete for EGFR-JM binding in vitro. a) MST data of the interaction of CaM and EGFR-ICD. Removal of accessible calcium via EGTA (black) as well as deletion of the first 27 residues of the JM segment (grey) largely reduces the binding of calcium-activated CaM to EGFR-ICD (green; n=3, mean+/-SD). b) Changes in EGFR-JM residue specific peak volumes upon addition of CaM. Peak disappearance reports on interaction between the effected JM residues and CaM (NMR intermediate exchange regime). Grey labels indicate residues that were not observed. c) MST data of the interaction between ARNO-Sec7 and EGFR-ICD in the absence (blue) or presence of 30 μM CaM (green; n=3, mean+/-SD). d) Schematic comparison of the observed CaM and Sec7 binding behavior of EGFR-JM.

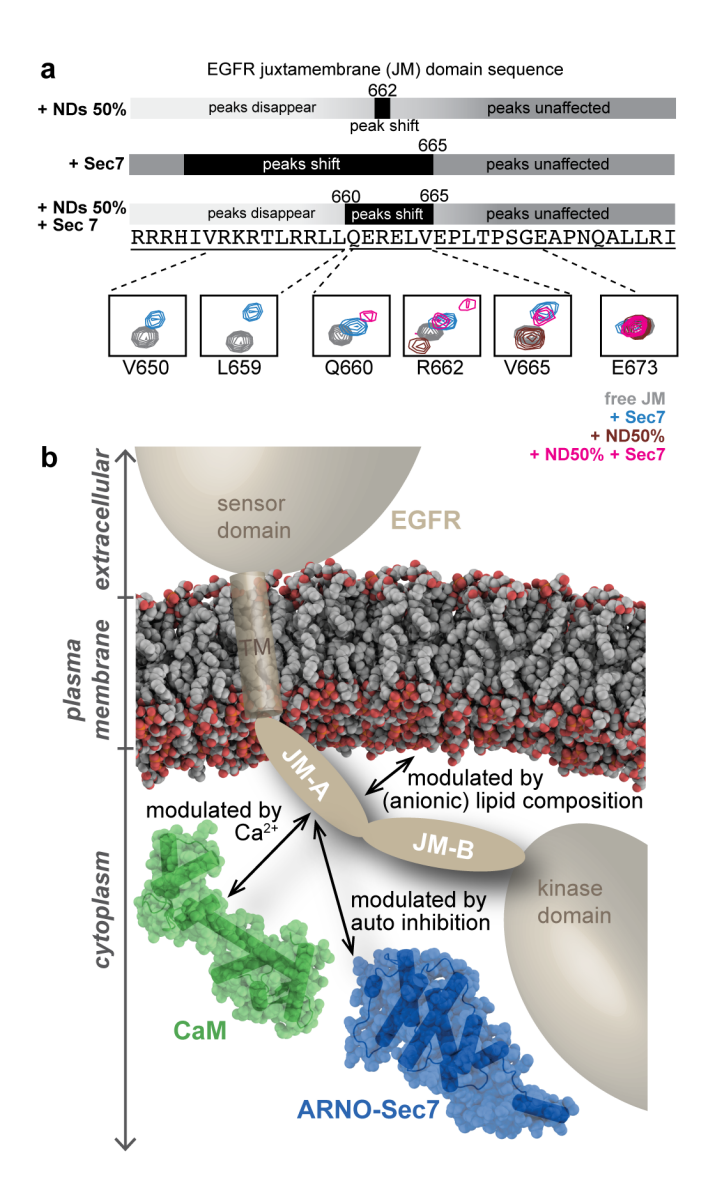


Fig. 5. The interplay between possible modulators acting on EGFR-JM as central interface in the intracellular interaction network of the EGFR. a) Comparison of NMR results for EGFR-JM in the presence of NDs with 50% anionic lipids (POPS, top), or in the presence of ARNO-Sec7 (middle), or in the presence of both interaction partners (lower schematic). Overlay of residue specific NMR signals in the absence (grey) or presence of indicated interaction partner(s). Selected residues, representative of the three differently affected regions, are shown. b) Schematic summary of EGFR-JM interaction partners, shown in this study to interact with the JM-A segment in vitro, and their individual modulators.

2D	Number of points			Spectral width (ppm)			Central frequency (ppm)			NC
	F3	F2	F1	F3	F2	F1	F3	F2	F1	NS
¹H,¹⁵N-TrHSQC	-	2048	128	-	14	36	-	4.704	116	64
3D										
TrHNCO	2048	40	128	14	36	22	4.704	116	176	8
TrHN(CA)CO	2048	40	128	14	36	22	4.704	116	176	24
TrHN(CO)CACB	2048	40	128	14	36	75	4.704	116	39	24
TrHNCACB	2048	40	128	14	36	75	4.704	116	39	32

**Table 2.** Acquisition parameters of the spectra used for JM resonance assignment.

2D	Number of points			Spectral width (ppm)			Central frequency (ppm)			NS
	F3	F2	F1	F3	F2	F1	F3	F2	F1	_ 143
<sup>1</sup> H, <sup>15</sup> N-HSQC	-	2048	256	-	13	30	-	4.697	119.5	32
<sup>1</sup> H, <sup>13</sup> C-HSQC	-	1024	512	-	13	75	-	4.696	42	32
3D										
HNCO	2048	40	128	13	30	22	4.697	119.5	176	8
HN(CA)CO	2048	40	128	13	30	22	4.697	119.5	176	16
CBCB(CO)NH	2048	40	128	13	30	80	4.697	119.5	42	32
HNCACB	2048	40	128	13	30	75	4.697	119.5	42	32
hCCH-TOCSY	2048	40	128	13	75	75	4.697	42	42	16

# 

## **STAR Methods**

### LEAD CONTACT AND MATERIALS AVAILABILITY

Further information and requests for resources and reagents should be directed to and will be fulfilled by the Lead Contact, Manuel Etzkorn (manuel.etzkorn@hhu.de). This study did not generate new unique reagents.

# 

#### **EXPERIMENTAL MODEL AND SUBJECT DETAILS**

All experiments were carried out with purified proteins (vide infra). No computational model was created.

# 

### **METHOD DETAILS**

Protein constructs and expression. Human EGFR-ICD (amino acids 645-1186, numbering according to UniProt P00533 without the 24 amino acids of the signal peptide) was equipped with a 6xHis tag and a TEV cleavage site and cloned into pFastBac-1 (Invitrogen) such that after TEV cleavage the protein contained two additional amino acids (Gly, Ala) at the *N-terminus*. EGFR-ICDΔJM<sub>1-27</sub> (amino acids 672-1186) was constructed by inserting a TEV cleavage site between amino acids 671 and 672 of EGFR-ICD and cloned into pACEBac-1 (ATG:biosynthetics) such that after TEV cleavage the protein had no additional amino acids. Recombinant baculoviruses were generated using the MultiBacTurbo Expression System

(ATG:biosynthetics) and proteins expressed for 3 days in SF9 cells (Invitrogen). EGFR-JM (amino acids 645-682) was fused to maltose binding protein followed by a TEV site such that after TEV cleavage the unmodified JM peptide was obtained. It was cloned into pET-28a (Novagen) and expressed for 3 h at 37 °C in *E. coli* BL21(DE3) (Stratagene). EGFR-JM<sub>SC</sub> was obtained by scrambling amino acids 645-682 resulting in the sequence: RELKHIQVRL RTERQLEPLE IRAVNRSRLT PRLAGLPR. Otherwise it was treated the same way. Human ARNO (UniProt Q99418), ARNOΔpbr (amino acids 1-386), ARNO-Sec7 (amino acids 61-246), ARNO-Sec7(4A) (Y186, F190, I193 and M194 changed to Ala) and human CaM (UniProt PODP23, amino acids 2-149) were equipped with a 6xHis tag and a TEV cleavage site, cloned into pET-28a and expressed at 20 °C overnight in *E. coli* BL21(DE3). Except for CaM, the constructs contain additional Gly and Ser at the *N-terminus* after TEV cleavage.

> Protein purification and labeling. All cell pellets were homogenized via French press in lysis buffer (50 mM Tris/HCl, pH 7.8, 300 mM NaCl, 10 % glycerol, 25 mM imidazole), except for calmodulin in different lysis buffer (50 mM HEPES/KOH, pH 7.8, 300 mM NaCl, 10 % glycerol, 25 mM imidazole). EGFR-ICD, EGFR-ICDΔJM<sub>1-27</sub>, all ARNO constructs and calmodulin were purified via Ni-NTA affinity chromatography (Macherey-Nagel). Eluted samples were buffer exchanged to remove imidazole, before TEV cleavage overnight at 4 °C. Protein samples were then subjected to reverse Ni-NTA chromatography (Macherey-Nagel), and concentrated using Vivaspin Turbo (Sartorius) followed by size exclusion chromatography either on HiLoad 16/600 Superdex 200pg (GE Healthcare) for EGFR-ICD and EGFR-ICDΔJM<sub>1-27</sub>, or on HiLoad 16/600 Superdex 75pg (GE Healthcare) for ARNO-Sec7, ARNO-Sec7(4A) and calmodulin. In addition, during TEV cleavage of EGFR-ICD, 0.5 μM His-tagged YopH and 0.5 mM MgCl<sub>2</sub> was added for dephosphorylation of the kinase. During calmodulin purification, cleared lysate was heated for 5 min at 80 °C, then cooled down on ice for 10 min, followed by centrifugation to remove denatured proteins. Furthermore, 1 mM of CaCl<sub>2</sub> was supplemented to the sample immediately before size exclusion chromatography. MBPT-EGFR-JM and MBPT-EGFR-JM<sub>SC</sub> were purified via amylose affinity chromatography (New England Biolabs), followed by TEV cleavage at room temperature for 48 h. Afterwards, digested sample was applied to size exclusion chromatography on HiLoad 16/600 Superdex 30pg (GE Healthcare). All the gel filtration runs were monitored at 280 nm, except for EGFR-JM, EGFR-JM<sub>SC</sub> and calmodulin at 214 nm. All the collected peak samples were concentrated in buffer H (20 mM HEPES/KOH, pH 7.8, 150 mM NaCl), using Vivaspin Turbo (Sartorius). For the fluorescence labeling of ARNO-Sec7 and ARNO-Sec7(4A), 10 μM proteins were mixed with 100 μM Alexa Fluor 647 NHS Ester (Thermo Fisher) in labeling buffer T (20mM HEPES/KOH, pH 7.8, 150 mM NaCl, 100 mM NaHCO₃). The labeling reactions were carried out on ice in the dark for 1 h. For the labeling of EGFR-ICD and EGFR-ICDΔJM<sub>1-27</sub>, 10 μM proteins were

MST measurements. For each MST assay, unlabeled protein was used to prepare 15-step serial dilution with final volume of 5  $\mu$ L in assay buffer (20 mM HEPES/KOH, pH 7.8, 150 mM NaCl, 0.005 % Triton X-100, 10  $\mu$ M BSA). Next, 5  $\mu$ L of 200 nM fluorescence-labeled protein was added to each dilution. For measurements including CaM (except for that with EGTA), 2 mM CaCl<sub>2</sub> was added to the assay buffer. The calmodulin titration was carried out in 1:2 serial dilution, while the others were performed in 1:3 dilution. For the calmodulin competition assay, 30  $\mu$ M calmodulin was premixed with 200 nM labeled

mixed with 30 μM RED-NHS 2nd generation (NanoTemper) in labeling buffer N (20 mM HEPES/KOH, pH 7.8, 150 mM NaCl).

The mixture was incubated on ice in darkness for 30 min. All labeling reactions were terminated by addition of 100 mM

Tris/HCl, pH 8. Afterwards, samples were applied to pre-equilibrated illustra Nap-5 columns (GE Healthcare) to remove free

dye, followed by elution with buffer H. Protein concentrations and degrees of labeling were quantified on NanoDrop 2000c

Spectrophotometer (Thermo Fisher), before aliquoting and flash freezing.

protein, before being added to 15 serial dilutions. Mixed samples were loaded into Monolith NT.115 Premium Capillaries (NanoTemper) and MST measurements were performed on Monolith NT.115 system (NanoTemper). For assays using labeled ARNO-Sec7 and ARNO-Sec7(4A), samples were pre-incubated at room temperature for 10 min and measured with 60 % LED power, 50 % MST power. For assays using labeled EGFR-ICD and EGFR-ICD $\Delta$ JM<sub>1-27</sub>, samples were pre-incubated at room temperature for 5 min and measured with 20 % LED power, 40 % MST power. Each sample preparation and measurement was carried out in triplicate. Data analysis was performed using the  $K_D$  fitting function of MO.Affinity Analysis v2.3 (NanoTemper) and graphs were prepared using Prism 5.0f (GraphPad). For the calculation of  $F_{norm}$ , hot cursor was set at 5 seconds for assays involving labeled ARNO-Sec7 and ARNO-Sec7(4A), while for assays involving labeled EGFR-ICD and EGFR-ICD $\Delta$ JM<sub>1-27</sub>, hot cursor was set at 2.5 seconds.

Nanodiscs production. Membrane scaffold protein expression and purification - As reported before (Bayburt et al., 1998), *E. coli* BL21 (DE3) were transformed with MSP1D1 plasmid DNA in vector pET28a. Cells were grown in LB medium, induced by 1 mM IPTG at an optical density of 0.7, incubated 5-6 hours at 37 °C and pelleted down. Cells were resuspended in buffer B (50 mM Tris/HCl, pH 8.0, 500 mM NaCl) supplemented with 6 M GdnHCl and EDTA-free Complete protease inhibitors (Roche) lysed by sonication (Bandelin Sonopuls MS72 probe), centrifuged at 17000·*g* for 1 h (Beckman J2-21 rotor JA-20.1) and incubated 1 h with previously equilibrated 2.5 ml Ni-NTA agarose resin/3 L culture (Macherey-Nagel). Column was washed with 4 CV buffer B, 4 CV buffer B supplemented with 1% Triton X-100, 4 CV buffer B + 60 mM Na-cholate, 4 CV buffer B, 4 CV buffer B + 20 mM imidazole. Four fractions of 1 CV were eluted with 250 mM imidazole. The whole process was kept at 4°C in a cold room. The elution fractions were pooled and dialyzed against 100-fold dialysis buffer (200 mM Tris/HCl, pH 7.5, 100 mM NaCl). N-terminal His-tag was cleaved using TEV protease incubated overnight at 4 °C. ΔHis-MSP was separated from MSP by IMAC and concentrated to the desired molarity using a Vivaspin centrifugal device of 10 kDa MWCO.

Nanodiscs assembly - Nanodiscs were assembled according to established protocols (Denisov et al., 2004; Ritchie et al., 2009). In short, lipids' chloroform stocks were dried under nitrogen flow to obtain a lipid film and stored under vacuum overnight. ΔHis-MSP1D1 and the appropriate amount of lipids (Avanti Polar Lipids) solubilized in 60 mM Na-cholate were mixed together in lipid buffer (20 mM Tris/HCl, pH 7.5, 100 mM NaCl, 5 mM EDTA). Four different batches were prepared: one using 100% 1-palmitoyl-2-oleoyl-sn-glycero-3-phosphocholine (POPC) as a non-charged control; one using 30% 1-palmitoyl-2-oleoyl-snglycero-3-phospho-L-serine (POPS) and 70% POPC containing 30% net negative charge and similar properties as native membranes; one using 50% POPS and 50% POPC with a higher density of negative charges; one using 50% 1,2-dimyristoylsn-glycero-3-phospho-(1'-rac-glycerol) (DMPG) and 50% 1,2-dimyristoyl-sn-glycero-3-phosphocholine (DMPC) containing 50% negative charge and different head group and hydrocarbon chain properties (see main text for more information). The scaffold-to-lipids molar ratio was calculated from geometrical considerations. 20% w/v of previously washed Biobeads SM-2 (Biorad) were added and the mixture incubated at room temperature overnight. The Biobeads were removed by centrifugation and once again 20% w/v were added for an additional 4-5 h. Finally, they were purified by SEC on a HiLoad 16/600 Superdex 200 pg column (GE Healthcare) equilibrated with SEC buffer (20 mM sodium phosphate, pH 7.4, 50 mM NaCl) using a Äkta pure device at a flow rate of 1 ml/min. The quality of NDs preparation was check by the SEC chromatogram as well as by DLS (PSS Nicomp). NDs were concentrated to the desired molarity using a Vivaspin centrifugal device of 10 kDa MWCO.

**NMR Spectroscopy.** All NMR experiments were performed on Bruker Avance III HD<sup>+</sup> spectrometers operating either at 600 or 700 MHz, both equipped with 5 mm inverse detection triple-resonance z-gradient cryogenic probes. Data was collected at 32 or 15°C and processed with TOPSPIN 3.2 (Bruker BioSpin). 4,4-dimethyl-4-silapentanesulfonic acid (DSS) was used as a chemical shift standard, and <sup>13</sup>C and <sup>15</sup>N data were referenced using frequency ratios as previously described (Wishart et al., 1995).

Sec7 and JM resonance assignment – For the resonance assignment of Sec7 and JM, triple (U[ $^2$ H, $^{13}$ C, $^{15}$ N]) and double-labelled ( $^{13}$ C, $^{15}$ N) samples were prepared, respectively. The U[ $^2$ H, $^{13}$ C, $^{15}$ N]-Sec7 sample was prepared at a concentration of 360 μM in 20 mM sodium phosphate buffer pH 7.4 containing 300 mM NaCl, 10% ( $^{v}$ V) D $_2$ O, 0.01% sodium azide and 100 μM DSS. The  $^{13}$ C, $^{15}$ N-JM sample was prepared at a concentration of 270 μM in 20 mM sodium phosphate buffer pH 5.5 containing 100 mM NaCl, 10% ( $^{v}$ V) D $_2$ O, 0.01% sodium azide and 100 μM DSS. The lower pH in this sample was used in order to avoid residue-amide exchange with the solvent. TROSY versions (Tr) of  $^{15}$ N-edited HSQC and three-dimensional HNCO, HN(CA)CO, HN(CO)CACB (or CBCA(CO)NH, for JM) and HNCACB experiments were performed to obtain the chemical shift assignments of the backbone atoms of Sec7, while the standard versions were used for JM. Furthermore, for the assignment of the sidechain resonances of JM we also acquired a  $^{13}$ C-edited HSQC and a 3D hCCH-TOCSY.

The assignment of the <sup>1</sup>H, <sup>13</sup>C, and <sup>15</sup>N signals in the spectra was performed using CARA 1.9.24a (Keller, 2004). Data was acquired at 32 and 15°C for U[<sup>2</sup>H,<sup>13</sup>C,<sup>15</sup>N]-Sec7 and <sup>13</sup>C,<sup>15</sup>N-JM, respectively. Tables 1 and 2 summarize the acquisition parameters for Sec7 and JM, respectively.

Sec7 titration with JM - The residues of Sec7 responsible for binding were identified by titrating a sample of  $^{15}$ N-labeled Sec7 with increasing amounts of non-labeled JM and acquiring a  $^{1}$ H, $^{15}$ N-HSQC spectrum at each titration point. The concentration of protein was maintained at 60 μM and the concentration of JM varied from 0 to 420 μM (using seven individual samples at 0.0, 0.5, 1.0, 2.0, 3.0, 5.0 and 7.0 molar equivalents). The  $^{1}$ H, $^{15}$ N-HSQC spectra were acquired with 2048 × 128 points and 256 scans. Spectral widths were 14 ppm for  $^{1}$ H and 36 ppm for  $^{15}$ N. The central frequency for proton was set on the solvent signal (4.704 ppm) and for nitrogen was set on the center of the amide region (116 ppm). The data was acquired in 20 mM sodium phosphate buffer containing 100 mM NaCl, 10% (v/v)  $D_2O$ , 0.01% sodium azide and 100 μM DSS, pH 7.4. All data was acquired at 32°C.

JM titration with Sec7, NDs and CaM - The residues of JM responsible for binding were identified in a similar way as described above, using  $^{15}$ N-labeled JM and non-labeled Sec7. The concentration of JM was maintained at 40 μM and the concentration of Sec7 varied from 0 to 280 μM (using five individual samples at 0.0, 2.0, 3.0, 5.0 and 7.0 molar equivalents). The  $^{1}$ H,  $^{15}$ N-HSQC spectra were acquired with 2048 × 128 points and 8 scans. Spectral widths were 13 ppm for  $^{1}$ H and 30 ppm for  $^{15}$ N. The central frequency for proton was set on the solvent signal (4.695 ppm) and for nitrogen was set on the center of the amide region (119.5 ppm). The data was acquired in 20 mM sodium phosphate buffer containing 100 mM NaCl, 10% (v/v) D<sub>2</sub>O, 0.01% sodium azide and 100 μM DSS, pH 5.5. All data was acquired at 15 and 32°C.

To study the interaction of JM with the different NDs we measured  $^{15}$ N-edited HSQC spectra of the free  $^{15}$ N-JM (40  $\mu$ M) and in the presence of 20  $\mu$ M of NDs, containing the different lipids (note that this will result on average in one JM per membrane leaflet). The  $^{1}$ H,  $^{15}$ N-HSQC spectra were acquired with 2048 × 128 points and 8 scans. Spectral widths were 15 ppm for  $^{1}$ H and 30 ppm for  $^{15}$ N. The central frequency for proton was set on the solvent signal (4.703 ppm) and for nitrogen was set on the

center of the amide region (119.5 ppm). The data was acquired in 20 mM sodium phosphate buffer containing 100 mM NaCl, 10% (v/v)  $D_2O$ , 0.01% sodium azide and 100  $\mu$ M DSS, pH 5.5. All data was acquired at 32°C.

The interaction between JM and calmodulin (CaM) was measured using  $^{15}$ N-edited HSQC experiments with 100  $\mu$ M  $^{15}$ N-labeled JM in absence and presence of 400  $\mu$ M CaM in 20 mM sodium phosphate buffer, pH 5.5, with 150 mM NaCl, 10% (v/v) D<sub>2</sub>O, 0.01% sodium azide and 100  $\mu$ M DSS. The spectra were acquired with 2048 x 128 points and the central frequency for protons were set on the solvent signal (4.690 ppm) and for nitrogens on 119.5 ppm. The spectral widths for  $^{1}$ H and  $^{15}$ N were set to 13 ppm and 30 ppm, respectively. Both spectra were acquired with 16 scans at 15 °C.

Data for JM's three N-terminal Arginines was not unambiguous and, where shown, could reflect either only on Arg647 or also on Arg646 and/or Arg645. Signal for His648 was considerably weaker as for all other assigned residues and not always clearly distinguishable from spectral noise. In unclear cases, the residue was removed from analysis.

JM<sub>SC</sub> titration with Sec7 – To investigate the effect of the overall charge of JM in binding we prepared a scrambled version of JM, JM<sub>SC</sub>, containing a redistributed but overall identical amino acid composition with the sequence: RELKHIQVRLRTERQLEPLEIRAVNRSRLTPRLAGLPR (positively and negatively charged residues are colored in blue and red, respectively).

We measured a  $^{15}$ N-edited HSQC spectrum of the free JMsc (40  $\mu$ M) and in the presence of 7.0 equivalents of Sec7 (280  $\mu$ M). The  $^{1}$ H,  $^{15}$ N-HSQC spectra were acquired with 2048  $\times$  128 points and 8 scans. Spectral widths were 13 ppm for  $^{1}$ H and 30 ppm for  $^{15}$ N. The central frequency for proton was set on the solvent signal (4.701 ppm) and for nitrogen was set on the center of the amide region (119.5 ppm). The data was acquired in 20 mM sodium phosphate buffer containing 100 mM NaCl, 10% (v/v) D<sub>2</sub>O, 0.01% sodium azide and 100  $\mu$ M DSS, pH 5.5. All data was acquired at 32°C.

**Combined Chemical Shift,**  $\Delta\delta_{comb}$ . For the evaluation of the behavior of individual amino acids upon addition of increasing amounts of ligand we calculated the combined amide proton and nitrogen chemical shift differences using Eq. 1 (Schumann et al., 2007):

$$\Delta \delta_{comb} = \sqrt{(\Delta \delta_H)^2 + (0.1 \times \Delta \delta_N)^2} \tag{1}$$

where  $\Delta \delta_H$  and  $\Delta \delta_N$  are the chemical shifts of proton and nitrogen, respectively. In order to decide whether a given residue belongs to the class of interacting or non-interacting residues, we have calculated a corrected standard deviation to zero  $(\sigma_0^{\text{corr}})$  (Schumann et al., 2007).

**Sec7 and JM Resonance Assignment.** Despite existence of an NMR structure of Sec7 (Betz et al., 1998), the experimental assignments are not available. As such, a *de novo* assignment was carried out. The backbone assignment of the amide resonances of Sec7 and JM has been performed using a standard triple resonance approach (Yamazaki et al., 1994). For Sec7, the amide resonances of amino acids S1, E2, T3, R4, Q5, R6, Y44, G48, K51, T52, F73, D74, L75, H76, R88, S93, F94, R95, L96, A100, Q101, K102, I103, D104, R105, M106, T125, N144, R148, D149 and L150 could not be assigned (possibly due to exchange with the solvent). The Chemical Shift Index (CSI) (Wishart et al., 1992) was used to identify protein secondary

structure and compare it with the deposited structures (Betz et al., 1998; Rouhana et al., 2013) (Fig. S1). The secondary structure of Sec7 was predicted for each assigned amino acid residue using Eq. 2:

533 534

531

532

$$CSI = \Delta \delta C_{\alpha} - \Delta \delta C_{\beta} \tag{2}$$

535 536

where CSI is the Chemical shift index and  $\Delta\delta C_{\alpha}$  and  $\Delta\delta C_{\beta}$  are the variations of the measured  $C_{\alpha}$  and  $C_{\beta}$  chemical shifts with respect to random coil values. Three or more consecutive negative values indicate  $\theta$ -strand while three or more positive values indicate a  $\alpha$ -helical structure.

539 540

537

538

541

542

**Structural solution and model validation.** No new structure was solved in this study. The existing structure of Sec7 (Betz et al., 1998; Rouhana et al., 2013) was validated via de novo NMR resonance assignments confirming the expected secondary structure elements (Fig. S1).

543 544

#### **QUANTIFICATION AND STATISTICAL ANALYSIS**

MST-data was recorded in triplicates for each conditions and respective statistical details are included in the methods details section as well as in the figure captions of each data plot. No statistical approach for assumption validation was used.

546 547

548

549

545

### **DATA AND CODE AVAILABILITY**

NMR chemical shift assignment of Sec7 are deposited in the BMRB data bank under the number: 27761.

550 551 552

553

### References

- Abd Halim, K.B., Koldsø, H., and Sansom, M.S.P. (2015). Interactions of the EGFR juxtamembrane domain with PIP<sub>2</sub>-containing lipid bilayers: Insights from multiscale molecular dynamics simulations. Biochim Biophys Acta *1850*, 1017-1025.
- Aifa, S., Johansen, K., Nilsson, U.K., Liedberg, B., Lundstrom, I., and Svensson, S.P.S. (2002). Interactions between the juxtamembrane domain of the EGFR and calmodulin measured by surface plasmon resonance. Cell Signal *14*, 1005-1013.
- Arkhipov, A., Shan, Y., Das, R., Endres, N.F., Eastwood, M.P., Wemmer, D.E., Kuriyan, J., and Shaw, D.E. (2013). Architecture and membrane interactions of the EGF receptor. Cell *152*, 557-569.
- Bayburt, T.H., Carlson, J.W., and Sligar, S.G. (1998). Reconstitution and imaging of a membrane protein in a nanometer-size phospholipid bilayer. J Struct Biol *123*, 37-44.
- Berjanskii, M.V., and Wishart, D.S. (2017). Unraveling the meaning of chemical shifts in protein NMR. Biochim Biophys Acta Proteins Proteom *1865*, 1564-1576.
- Betz, S.F., Schnuchel, A., Wang, H., Olejniczak, E.T., Meadows, R.P., Lipsky, B.P., Harris, E.A., Staunton, D.E., and Fesik, S.W. (1998). Solution structure of the cytohesin-1 (B2-1) Sec7 domain and its interaction with the GTPase ADP ribosylation factor
- 1. Proc Natl Acad Sci U S A *95*, 7909-7914.
- Bill, A., Schmitz, A., Konig, K., Heukamp, L.C., Hannam, J.S., and Famulok, M. (2012). Anti-proliferative effect of cytohesin inhibition in gefitinib-resistant lung cancer cells. PloS one *7*, e41179.
- Cai, G., Zhu, L., Chen, X., Sun, K., Liu, C., Sen, G.C., Stark, G.R., Qin, J., and Li, X. (2018). TRAF4 binds to the juxtamembrane region of EGFR directly and promotes kinase activation. Proc Natl Acad Sci U S A *115*, 11531-11536.
- 571 Cherfils, J., Menetrey, J., Mathieu, M., Le Bras, G., Robineau, S., Beraud-Dufour, S., Antonny, B., and Chardin, P. (1998).
  572 Structure of the Sec7 domain of the Arf exchange factor ARNO. Nature *392*, 101-105.

- 573 Choowongkomon, K., Carlin, C.R., and Sonnichsen, F.D. (2005). A structural model for the membrane-bound form of the
- juxtamembrane domain of the epidermal growth factor receptor. J Biol Chem 280, 24043-24052.
- 575 Citri, A., and Yarden, Y. (2006). EGF-ERBB signalling: towards the systems level. Nat Rev Mol Cell Biol 7, 505-516.
- 576 Cochet, C., Gill, G.N., Meisenhelder, J., Cooper, J.A., and Hunter, T. (1984). C-kinase phosphorylates the epidermal growth
- factor receptor and reduces its epidermal growth factor-stimulated tyrosine protein kinase activity. J Biol Chem 259, 2553-
- 578 **2558**.
- 579 Cohen, L.A., Honda, A., Varnai, P., Brown, F.D., Balla, T., and Donaldson, J.G. (2007). Active Arf6 recruits ARNO/cytohesin
- GEFs to the PM by binding their PH domains. Mol Biol Cell 18, 2244-2253.
- Davis, R.J., and Czech, M.P. (1985). Tumor-promoting phorbol diesters cause the phosphorylation of epidermal growth factor
- receptors in normal human fibroblasts at threonine-654. Proc Natl Acad Sci U S A 82, 1974-1978.
- Denisov, I.G., Grinkova, Y.V., Lazarides, A.A., and Sligar, S.G. (2004). Directed self-assembly of monodisperse phospholipid
- bilayer nanodiscs with controlled size. J Am Chem Soc 126, 3477-3487.
- DiNitto, J.P., Delprato, A., Gabe Lee, M.T., Cronin, T.C., Huang, S., Guilherme, A., Czech, M.P., and Lambright, D.G. (2007).
- 586 Structural basis and mechanism of autoregulation in 3-phosphoinositide-dependent Grp1 family Arf GTPase exchange
- factors. Mol Cell 28, 569-583.
- Doerner, A., Scheck, R., and Schepartz, A. (2015). Growth factor identity is encoded by discrete coiled-coil rotamers in the
- EGFR juxtamembrane region. Chem Biol 22, 776-784.
- 590 Endres, N.F., Das, R., Smith, A.W., Arkhipov, A., Kovacs, E., Huang, Y., Pelton, J.G., Shan, Y., Shaw, D.E., Wemmer, D.E., et al.
- (2013). Conformational coupling across the plasma membrane in activation of the EGF receptor. Cell 152, 543-556.
- 592 Friedman, B., Frackelton, A.R., Ross, A.H., Connors, J.M., Fujiki, H., Sugimura, T., and Rosner, M.R. (1984). Tumor promoters
- block tyrosine-specific phosphorylation of the epidermal growth factor receptor. Proc Natl Acad Sci U S A 81, 3034-3038.
- He, L., and Hristova, K. (2012). Consequences of replacing EGFR juxtamembrane domain with an unstructured sequence.
- 595 Scientific reports 2, 854.
- Hedger, G., Sansom, M.S., and Koldso, H. (2015). The juxtamembrane regions of human receptor tyrosine kinases exhibit
- conserved interaction sites with anionic lipids. Scientific reports 5, 9198.
- Hunter, T., Ling, N., and Cooper, J.A. (1984). Protein kinase C phosphorylation of the EGF receptor at a threonine residue
- close to the cytoplasmic face of the plasma membrane. Nature *311*, 480-483.
- Jura, N., Endres, N.F., Engel, K., Deindl, S., Das, R., Lamers, M.H., Wemmer, D.E., Zhang, X., and Kuriyan, J. (2009). Mechanism
- for activation of the EGF receptor catalytic domain by the juxtamembrane segment. Cell 137, 1293-1307.
- Keller, R. (2004). The computer aided resonance assignment tutorial. In Institute for Molecular Biology and Boiphysics (Zurich:
- The Swiss Federal Institute of Technology), ISBM 3-85600-112-3.
- 604 Kovacs, E., Zorn, J.A., Huang, Y., Barros, T., and Kuriyan, J. (2015). A structural perspective on the regulation of the epidermal
- growth factor receptor. Annu Rev Biochem 84, 739-764.
- 606 Lemmon, M.A., Schlessinger, J., and Ferguson, K.M. (2014). The EGFR family: not so prototypical receptor tyrosine kinases.
- 607 Cold Spring Harbor Perspectives in Biology 6, a020768.
- Li, H., Panina, S., Kaur, A., Ruano, M.J., Sánchez-González, P., la Cour, J.M., Stephan, A., Olesen, U.H., Berchtold, M.W., and
- 609 Villalobo, A. (2012). Regulation of the Ligand-dependent Activation of the Epidermal Growth Factor Receptor by Calmodulin.
- J Biol Chem 287, 3273-3281.
- 611 Li, X., Huang, Y., Jiang, J., and Frank, S.J. (2008). ERK-dependent threonine phosphorylation of EGF receptor modulates
- receptor downregulation and signaling. Cell Signal 20, 2145-2155.
- Maeda, R., Sato, T., Okamoto, K., Yanagawa, M., and Sako, Y. (2018). Lipid-protein interplay in dimerization of juxtamembrane
- domains of epidermal growth factor receptor. Biophys J 114, 893-903.
- Martin-Nieto, J., and Villalobo, A. (1998). The human epidermal growth factor receptor contains a juxtamembrane
- calmodulin-binding site. Biochemistry *37*, 227-236.
- McLaughlin, S., Smith, S.O., Hayman, M.J., and Murray, D. (2005). An electrostatic engine model for autoinhibition and
- activation of the epidermal growth factor receptor (EGFR/ErbB) family. J Gen Physiol *126*, 41-53.

- Michailidis, I.E., Rusinova, R., Georgakopoulos, A., Chen, Y., Iyengar, R., Robakis, N.K., Logothetis, D.E., and Baki, L. (2011).
- Phosphatidylinositol-4,5-bisphosphate regulates epidermal growth factor receptor activation. Pflugers Arch 461, 387-397.
- 621 Mineev, K.S., Panova, S.V., Bocharova, O.V., Bocharov, E.V., and Arseniev, A.S. (2015). The membrane mimetic affects the
- spatial structure and mobility of EGFR transmembrane and juxtamembrane domains. Biochemistry 54, 6295-6298.
- Morrison, P., Takishima, K., and Rosner, M.R. (1993). Role of threonine residues in regulation of the epidermal growth factor
- receptor by protein kinase C and mitogen-activated protein kinase. J Biol Chem 268, 15536-15543.
- 625 Mossessova, E., Gulbis, J.M., and Goldberg, J. (1998). Structure of the guanine nucleotide exchange factor Sec7 domain of
- human arno and analysis of the interaction with ARF GTPase. Cell 92, 415-423.
- 627 Pan, T., Sun, J., Hu, J., Hu, Y., Zhou, J., Chen, Z., Xu, D., Xu, W., Zheng, S., and Zhang, S. (2014). Cytohesins/ARNO: the function
- in colorectal cancer cells. PloS one *9*, e90997.
- Pan, T., Sun, J., Zhou, J., Fu, Z., Hu, Y., Zheng, S., and Zhang, S. (2013). Function and mode of action of cytohesins in the
- epidermal growth factor pathway in colorectal cancer cells. Oncology letters 5, 521-526.
- Poppleton, H.M., Wiepz, G.J., Bertics, P.J., and Patel, T.B. (1999). Modulation of the protein tyrosine kinase activity and
- autophosphorylation of the epidermal growth factor receptor by its juxtamembrane region. Arch Biochem Biophys 363, 227-
- 633 **236**.
- Red Brewer, M., Choi, S.H., Alvarado, D., Moravcevic, K., Pozzi, A., Lemmon, M.A., and Carpenter, G. (2009). The
- iuxtamembrane region of the EGF receptor functions as an activation domain. Molecular Cell 34, 641-651.
- Ritchie, T.K., Grinkova, Y.V., Bayburt, T.H., Denisov, I.G., Zolnerciks, J.K., Atkins, W.M., and Sligar, S.G. (2009). Reconstitution
- of membrane proteins in phospholipid bilayer nanodiscs. In Methods Enzymol, D. Nejat, ed. (Elsevier Inc.), pp. 211-231.
- Rouhana, J., Hoh, F., Estaran, S., Henriquet, C., Boublik, Y., Kerkour, A., Trouillard, R., Martinez, J., Pugniere, M., Padilla, A., et
- 639 al. (2013). Fragment-based identification of a locus in the Sec7 domain of Arno for the design of protein-protein interaction
- inhibitors. J Med Chem 56, 8497-8511.
- 641 Sanchez-Gonzalez, P., Jellali, K., and Villalobo, A. (2010). Calmodulin-mediated regulation of the epidermal growth factor
- receptor. FEBS J 277, 327-342.
- 643 Sato, T., Pallavi, P., Golebiewska, U., McLaughlin, S., and Smith, S.O. (2006). Structure of the membrane reconstituted
- transmembrane-juxtamembrane peptide EGFR(622-660) and its interaction with Ca<sup>2+</sup>/calmodulin. Biochemistry 45, 12704-
- 645 **12714.**
- 646 Schumann, F.H., Riepl, H., Maurer, T., Gronwald, W., Neidig, K.P., and Kalbitzer, H.R. (2007). Combined chemical shift changes
- and amino acid specific chemical shift mapping of protein-protein interactions. J Biomol NMR 39, 275-289.
- Sengupta, P., Bosis, E., Nachliel, E., Gutman, M., Smith, S.O., Mihalyne, G., Zaitseva, I., and McLaughlin, S. (2009). EGFR
- juxtamembrane domain, membranes, and calmodulin: kinetics of their interaction. Biophys J 96, 4887-4895.
- 650 Stalder, D., Barelli, H., Gautier, R., Macia, E., Jackson, C.L., and Antonny, B. (2011). Kinetic studies of the Arf activator Arno on
- model membranes in the rresence of Arf effectors suggest control by a positive feedback loop. J Biol Chem 286, 3873-3883.
- Tebar, F., Villalonga, P., Sorkina, T., Agell, N., Sorkin, A., and Enrich, C. (2002). Calmodulin regulates intracellular trafficking of
- epidermal growth factor receptor and the MAPK signaling pathway. Mol Biol Cell 13, 2057-2068.
- Thiel, K.W., and Carpenter, G. (2007). Epidermal growth factor receptor juxtamembrane region regulates allosteric tyrosine
- kinase activation. Proc Natl Acad Sci U S A 104, 19238-19243.
- Viegas, A., Viennet, T., and Etzkorn, M. (2016). The power, pitfalls and potential of the nanodisc system for NMR-based
- studies. Biol Chem *397*, 1335-1354.
- Viennet, T., Wordehoff, M.M., Uluca, B., Poojari, C., Shaykhalishahi, H., Willbold, D., Strodel, B., Heise, H., Buell, A.K., Hoyer,
- 659 W., et al. (2018). Structural insights from lipid-bilayer nanodiscs link alpha-Synuclein membrane-binding modes to amyloid
- fibril formation. Commun Biol 1, 44.
- Wang, Y., Gao, J., Guo, X., Tong, T., Shi, X., Li, L., Qi, M., Wang, Y., Cai, M., Jiang, J., et al. (2014). Regulation of EGFR nanocluster
- formation by ionic protein-lipid interaction. Cell Res *24*, 959-976.
- 663 Wishart, D.S., Bigam, C.G., Yao, J., F., A., Dyson, H.J., Oldfield, E., Markley, J.L., and Sykes, B.D. (1995). 1H, 13C and 15N
- chemical shift referencing in biomolecular NMR. J Bio NMR 6.

- Wishart, D.S., Sykes, B.D., and Richards, F.M. (1992). The chemical shift index: a fast and simple method for the assignment of protein secondary structure through NMR spectroscopy. Biochemistry *31*, 1647-1651.
- Yamazaki, T., Lee, W., Arrowsmith, C.H., Muhandiram, D.R., and Kay, L.E. (1994). A suite of triple resonance NMR experiments for the backbone assignment of <sup>15</sup>N, <sup>13</sup>C, <sup>2</sup>H labeled proteins with high sensitivity. J Am Chem Soc *116*, 11655-11666.
- Zhang, X., Gureasko, J., Shen, K., Cole, P.A., and Kuriyan, J. (2006). An allosteric mechanism for activation of the kinase domain of epidermal growth factor receptor. Cell *125*, 1137-1149.